View metadata, citation and similar papers at core.ac.uk
brought to you by CORE
provided by Institute of Transport Research:Publications

CEAS Space J
DOI 10.1007/s12567-016-0124-6

ORIGINAL PAPER

Development of an innovative validation strategy of gas–surface interaction modelling for re-entry applications

N. Joiner[1] · B. Esser[2] · M. Fertig[3] · A. Gülhan[2] · G. Herdrich[4] · B. Massuti-Ballester[4]

Received: 17 September 2015 / Revised: 18 April 2016 / Accepted: 18 May 2016
© CEAS 2016

Abstract This paper summarises the final synthesis of an ESA technology research programme entitled "Development of an Innovative Validation Strategy of Gas Surface Interaction Modelling for Re-entry Applications". The focus of the project was to demonstrate the correct pressure dependency of catalytic surface recombination, with an emphasis on Low Earth Orbit (LEO) re-entry conditions and thermal protection system materials. A physics-based model describing the prevalent recombination mechanisms was proposed for implementation into two CFD codes, TINA and TAU. A dedicated experimental campaign was performed to calibrate and validate the CFD model on TPS materials pertinent to the EXPERT space vehicle at a wide range of temperatures and pressures relevant to LEO. A new set of catalytic recombination data was produced that was able to improve the chosen model calibration for CVD-SiC and provide the first model calibration for the Nickel–Chromium super-alloy PM1000. The experimentally observed pressure dependency of catalytic recombination can only be reproduced by the Langmuir–Hinshelwood recombination mechanism. Due to decreasing degrees of (enthalpy and hence) dissociation with facility stagnation pressure, it was not possible to obtain catalytic recombination coefficients from the measurements at high experimental stagnation pressures. Therefore, the CFD model calibration has been improved by this activity based on the low pressure results. The results of the model calibration were applied to the existing EXPERT mission profile to examine the impact of the experimentally calibrated model at flight relevant conditions. The heat flux overshoot at the CVD-SiC/PM1000 junction on EXPERT is confirmed to produce radiative equilibrium temperatures in close proximity to the PM1000 melt temperature.This was anticipated within the margins of the vehicle design; however, due to the measurements made here for the first time at relevant temperatures for the junction, an increased confidence in this finding is placed on the computations.

Keywords Aerothermodynamics · Catalytic recombination · CFD · High-enthalpy facilities

1 Introduction

During hypersonic entry into the Earth's atmosphere, the high temperatures developed behind the resulting bow shock are able to dissociate a large fraction of the molecular nitrogen and oxygen in the air. The energy required to break the chemical bonds results in a cooling effect in the shock layer. When the hot shock gases reach the relatively cool surface of a re-entry vehicle, the drop in temperature causes some of the atoms to recombine releasing energy into the boundary layer. Additional heating may also occur due to gas–surface chemical reactions; oxidation, for example, is almost exclusively exothermic. This effect may be exacerbated by catalytic behaviour of the surface material or the by-products of

This work was funded by ESA contract 4000103000. The authors would like to thank Domenico Giordano for his constructive comments and suggestions during the performance of this work.

✉ N. Joiner
nathan.joiner@fluidgravity.co.uk

[1] Fluid Gravity Engineering Ltd. (FGE), 1 West Street, PO10 7DX Emsworth, UK

[2] DLR, Linder Höhe, 51147 Köln, Germany

[3] DLR, Lilienthalplatz 7, 38108 Braunschweig, Germany

[4] IRS, University of Stuttgart, Pfaffenwaldring 29, 70569 Stuttgart, Germany

Published online: 28 May 2016

gas–surface reactions. The difference in heat loads on the vehicle surface, between non-catalytic recombination and the scenario of complete recombination, is large and, therefore, understanding the extent of the catalytic effect is very important for the design and evaluation of a thermal protection system (TPS) and ultimately mission success.

The catalycity of a surface is measured by the 'recombination coefficient' or 'catalytic efficiency' γ, defined as the ratio of the number of atoms recombining to the number of atoms reaching the surface. The recombination coefficient ranges between 0 (non-catalytic) and 1 (fully catalytic). A number of physical considerations can impact the effective recombination coefficient, including diffusion, surface roughness, and surface state.

The recombination coefficient of materials can be determined via a number of different methods and experimental facilities [8]. Plasma wind tunnels are one of the few facilities that can provide a wide range of pressure and material surface temperatures relevant to re-entry conditions simultaneously. Further, they can provide a reasonable steady-state flow, which can be tested with the same CFD codes that are employed in space vehicle design. Experimental campaigns to measure catalysis essentially measure the effective recombination coefficient, and typically fall into two types: those that measure concentrations of species and those that use energy balances to infer catalysis. The experiments performed under the current work obtain recombination coefficients using the latter method.

The content of this paper is arranged as follows: The methodology is described in the next chapter. This will introduce the catalytic CFD model employed in the study and the validation strategy as a whole. An overview of the direct method for extracting recombination coefficients from experimental data used in this work along with the synthesis from the PWK3 inductive facility and L2K arc-heated facility will then be provided, followed by a chapter presenting the consolidated outputs from CFD studies with the codes TAU and TINA. Finally, conclusions will be drawn, the main results, lessons learnt and difficulties will be summarised, and recommendations for future work and improvements to the method made.

2 Validation methodology

The aim of this activity was to measure the catalytic recombination coefficients of nitrogen and oxygen on materials relevant to LEO re-entry vehicles (with an emphasis on the EXPERT vehicle) at flight relevant temperatures and pressures. Then, use the data to calibrate and validate a catalysis model in the CFD codes TINA (FGE) and TAU (DLR). The priorities of this work are as follows:

- Perform tests at a wide range of pressures on flight materials
- Generate validation data for recombination coefficient models
- Validate the implemented CFD models against test data
- Determine the dominant catalytic mechanism for LEO applications
- Rebuild available EXPERT flight data or investigate the impact of the study on flight predictions

To achieve these goals, an emphasis is placed on the pressure dependency of the catalytic efficiency. Historically, this has often been overlooked in catalysis studies, and was identified in the work of Fertig et al. [5] as an important consideration for CFD model validation. Experiments performed by Kolesnikov et al. [11] at EXPERT relevant temperature and pressure conditions (170 and 540 hPa with surface temperatures in the range 1620–2030 K) on a SiC surface indicate that a pressure dependency of catalytic recombination efficiency can be observed. In these tests, there was only one common surface temperature (1620 K) tested between the two pressure conditions and it was found that there was no appreciable catalytic recombination for this temperature at 540hPa. The catalytic recombination rate is much more sensitive to temperature than pressure, and the pressure dependency (and dominant catalytic mechanism) may vary with temperature. It is, therefore, necessary to perform experimental tests at fixed surface temperature and vary the pressure, to identify the dominant catalytic mechanism from the test data. This is the underlying hypothesis of the validation campaign strategy.

2.1 Catalytic recombination model

As the CFD model has been detailed elsewhere [5], only a brief review of the main formulae is given here, in order to introduce the parameters used for model calibration in Sect. 4.1. Since the number of active sites where atoms can be bound to the surface for some time is assumed to be constant, it is convenient to introduce the surface coverage

$$\Theta_i = \frac{\tilde{n}_i}{\tilde{n}_0}, \tag{1}$$

which is the relation of the surface number density of adsorbed particles of species i to the total number density of active sites. The adsorption rate is given by

$$\tilde{\omega}_{Ad,i} = \tilde{n}_0 \pi \sigma_{Ad,i}^2 \Theta_z N_{n,i}^{(-)} \left(e^{-\frac{A_{Ad,i}}{\Re T}} - e^{-\frac{A_{Ad,i,max}}{\Re T}} \right), \tag{2}$$

where $\pi \sigma_{Ad,i}^2$ is the reactive cross section for adsorption and $N_{n,i}^{(-)}$ is the molar particle flux to the surface due to diffusion and collisional impact,

$$\Theta_z = 1 - \sum\nolimits_i \Theta_i \tag{3}$$

denotes the number of free active sites, and $A_{Ad,i}$, $A_{Ad,i,max}$ are the minimum and maximum energies for an adsorbing particle. The desorption rate is given by

$$\tilde{\omega}_{Des,i} = \frac{s_{Ad,i}(\Theta_z, T)}{\Theta_z} \sqrt{\frac{kT}{2\pi m_i}} \frac{Z_i}{Z_{Ad,i}} \frac{\tilde{n}_0}{N_A} \Theta_i e^{-\frac{D_{Des,i}}{\Re T}}, \tag{4}$$

where

$$s_{Ad,i}(\Theta_z, T) = \frac{\tilde{\omega}_{Ad,i}}{N_{n,i}^{(-)}} \tag{5}$$

is the so-called sticking coefficient, N_A is the Avogadro constant, and Z_i and $Z_{Ad,i}$ are the partition functions for free and adsorbed particles of species i. At least, one translational degree of freedom with the one-dimensional partition function

$$Z_{tr}(T) = \sqrt{\frac{2\pi m_i kT}{h^2}}, \tag{6}$$

where h is the Plancks constant, is transferred into a vibrational one due to adsorption. Employing a truncated harmonic oscillator model, the vibrational partition function can be expressed by

$$Z_{v,i}^{D_{Des,i}}(T) = \frac{1 - e^{-\frac{D_{Des,i}}{\Re T}}}{1 - e^{-\frac{\Theta_{v,i}}{\Re T}}}, \tag{7}$$

where $\Theta_{v,i}$ is the characteristic vibrational temperature. Under the assumption that the adsorbed atoms can move along the surface, one derives

$$\tilde{\omega}_{Des,i} = \frac{s_{Ad,i}(\Theta_z, T)}{\Theta_z} \frac{kT}{h} \frac{1}{Z_{v,i}^{D_{Des,i}}} \frac{\tilde{n}_0}{N_A} \Theta_i e^{-\frac{D_{Des,i}}{\Re T}} \tag{8}$$

for the desorption rate.

The recombination rate for non-adsorbed gas atoms with an adsorbed particle (Eley–Rideal mechanism [1]) is given by

$$\begin{aligned} \tilde{\omega}_{ER,ij} &= \tilde{n}_0 \pi \sigma_{ER,ij}^2 N_{n,i}^{(-)} \Theta_j e^{-\frac{A_{ER,ij}}{\Re T}} \\ &= c_{ER} N_{n,i}^{(-)} \Theta_j e^{-\frac{A_{ER,ij}}{\Re T}}, \end{aligned} \tag{9}$$

where $\pi \sigma_{ER,ij}^2$ and $A_{ER,ij}$ are the reactive cross section and the activation energy for the Eley–Rideal (ER) recombination of impinging particle i with adsorbed particle j.

The Langmuir–Hinshelwood (LH) mechanism [9, 12], which describes the recombination of two adsorbed atoms, is considered a high temperature mechanism, since activation energy is typically higher than that of the Eley–Rideal (ER) mechanism. The reaction rate is given by

$$\begin{aligned} \tilde{\omega}_{LH,ij} &= P_{Ster,LH,ij} \frac{kT}{h} \frac{1}{Z_{v,i}^{D_{Diff,i}}} \frac{\tilde{n}_0}{N_A} \Theta_i \Theta_j e^{-\frac{A_{LH,eff,ij}}{\Re T}} \\ &= \frac{c_{LH} T}{Z_{v,i}^{D_{Diff,i}}} \Theta_i \Theta_j e^{-\frac{A_{LH,eff,ij}}{\Re T}}, \end{aligned} \tag{10}$$

where the effective activation energy of the reaction is the sum of the diffusion energy and the activation energy for Eley–Rideal recombination.

Concurrent adsorption of different species at the same active sites requires the numerical solution of a coupled set of balance equations for the determination of the surface coverage. The recombination of a single type of atom allows for an analytic determination of the surface coverage, which is used within the model calibration procedure. Under steady-state conditions, the balance equation

$$\tilde{\omega}_{Ad,i} - \tilde{\omega}_{Des,i} - \tilde{\omega}_{ER,ii} - 2\tilde{\omega}_{LH,ii} = 0 \tag{11}$$

holds. This equation raises a simple quadratic equation for the determination of Θ_i. Hence, Θ_i can be determined via

$$\Theta_i = -a_{\Theta,i} + \sqrt{a_{\Theta,i}^2 + b_{\Theta,i}} \tag{12}$$

with

$$a_{\Theta,i} = \frac{\frac{\tilde{\omega}_{Ad,i}}{\Theta_i} + \frac{\tilde{\omega}_{Des,i}}{\Theta_Z} + \frac{\tilde{\omega}_{ER,ii}}{\Theta_i}}{4\frac{\tilde{\omega}_{LH,ii}}{\Theta_i^2}} \quad \text{and} \quad b_{\Theta,i} = \frac{\frac{\tilde{\omega}_{Ad,i}}{\Theta_i}}{2\frac{\tilde{\omega}_{LH,ii}}{\Theta_i^2}}. \tag{13}$$

The recombination coefficient for the recombination of a single species i is determined by

$$\gamma_i = 2\frac{\tilde{\omega}_{ER,ii} + \tilde{\omega}_{LH,ii}}{N_{n,i}^{(-)}}. \tag{14}$$

The pressure dependency in all the above equations enters through the surface particle flux $N_{n,i}^{(-)}$, which is directly proportional to the pressure, and the surface coverage. The surface coverage dependency in steady state is readily inferred from Eqs. 2 and 4. It is found that at low temperatures, the surface coverage is constant with pressure, and tends towards a linear dependence on pressure at high temperature. Considering then the resulting pressure dependency of the recombination coefficient due to the ER and LH mechanisms, it is apparent (from the recombination rate Eqs. 9 and 10, and the definition of the recombination coefficient) that at low temperature the ER recombination coefficient has no pressure dependency, while the LH recombination coefficient is inversely proportional to pressure. At sufficiently high temperatures, both mechanisms have recombination coefficients that increase monotonically with pressure. The different character of the recombination

Table 1 Temperature (T), stagnation pressure (P_{stag}) and heatflux ($\dot{q}$) ranges addressed at experimental facilities

Facility	T Range (K)	P_{stag} Range (Pa)	$\dot{q}$ Range (kW/m^2)
PWK3	1200–2000	100–4000	~100–5000
L2K	1200–1600	2000–20000	~100–500

coefficients at low temperature, therefore, allows the dominant mechanism to be distinguishable from pressure-dependent experimental catalytic data.

2.2 Experimental method

The choice of experimental facilities is primarily based on the requirement that flight relevant plasma conditions for LEO were obtained. The emphasis of the project was on the EXPERT mission. Surface temperatures of interest fall into the range of 1000 to 2000K, while relevant stagnation pressures are 1000 to 50,000 Pa. Experiments were conducted at the PWK3 inductive wind tunnel at IRS Stuttgart and L2K arc-heated wind tunnel at DLR Cologne. Material surface temperatures relevant to flight are easily obtained, and the lower part of the flight pressure range can be reproduced. PWK3 is used to provide model calibration data. L2K is able to produce temperatures and pressures representative of flight conditions, and has a history of accurate CFD reproduction of the plasma conditions in previous campaigns. L2K is, therefore, ideal to complement the CFD model calibration data from PWK3 and provide further data to be used exclusively for CFD model validation at higher pressures. The operating ranges of temperature and pressure in the facilities chosen for this study are given in Table 1.

The relevant materials for LEO return TPS application are Ultra High Temperature Ceramics (UHTCs) and metallics. Since EXPERT was scheduled to fly within the timeframe of the TRP, it was a likely candidate for flight data rebuilding. It was, therefore, an advantage to use the same materials as used on EXPERT in this campaign, thereby eliminating uncertainties in the material. The UHTC used on EXPERT is a C/C-SiC with a Chemical Vapour Deposited (CVD)-SiC coating. The material is produced by DLR in Stuttgart and was used in this study. A Nickel–Chromium super alloy called PM1000 is used on EXPERT; while this material is no longer manufactured, a quantity suitable for this campaign was procured.

The chosen conditions for the PWK3 inductive facility tests on CVD-SiC and PM1000 are given in Table 2. Each of the PWK3 test conditions was performed in both oxygen and nitrogen plasmas. The chosen conditions for the L2K arc-heater tests are given in Table 3. Each of the L2K test conditions was performed in both nitrogen and air plasmas.

Table 2 PWK3 inductive facility test matrix

Sample	Surface temperature (K)	Stagnation pressure (Pa)
CVD-SiC	1400	100
CVD-SiC	1400	500
CVD-SiC	1400	2000
PM1000	1500	100
PM1000	1500	500
PM1000	1500	2000

Nominal test conditions performed in both nitrogen and oxygen plasmas, for the purpose of CFD model calibration

The 1400 K wall temperature was chosen as a temperature expected at the junction between C/C-SiC and PM1000 under peak heating conditions. Moreover, measurements of Stewart [20] showed a maximum in recombination probability on SiC at around this temperature. The 1500 K temperature provides measurements of the catalytic efficiency closer to the melting point of PM1000 than measured before. The facility calibration strategy was to match the nominal surface temperatures as closely as possible, to allow for the determination of the dominant recombination mechanism, as catalytic recombination mechanisms are characterised by different pressure dependencies.

2.3 CFD validation methodology

The intended model verification and validation are achieved with direct comparisons of the catalytic recombination coefficient, and stagnation point values of temperature and pressure obtained in the L2K experiments. Experimental rebuilds occurred for the conditions given in Table 4 for both air and nitrogen plasmas. The underlying principle of the CFD validation methodology is as follows: the model is calibrated with the low pressure data and verified at a stagnation pressure of 2000 Pa (relevant to the EXPERT material junction); then applied to the high pressure (15,000 Pa) cases (relevant to the EXPERT stagnation region) to validate the correct extrapolation of the calibrated model to high pressure.

The 15,000 Pa L2K conditions were intended for validation only. It will be discussed in subsequent sections how the recombination coefficients of the 15,000 Pa stagnation pressure cases could not be obtained due to extremely low dissociation levels in the arc-heated facility (an implication, and anticipated risk, of the enthalpy required to obtain the material surface temperatures of interest). All other test points were intended for CFD model calibration, with the 2000 Pa L2K cases being rebuilt for verification purposes. If recombination coefficients at 15,000 Pa had been obtained, the validation could, in principle, show that the

Table 3 L2K arc-heater test matrix

Sample	Surface temperature (K)	Stagnation pressure (Pa)
CVD-SiC	1400	2000
CVD-SiC	1400	5000
CVD-SiC	1400	15,000
PM1000	1400	2000
PM1000	1400	5000
PM1000	1400	15,000
CVD-SiC	1600	2000
CVD-SiC	1600	5000
CVD-SiC	1600	15,000
PM1000	1500	2000
PM1000	1500	5000
PM1000	1500	15,000

Nominal test conditions performed in both nitrogen and air plasmas. Tests at 2000 and 5000 Pa are intended for CFD model calibration, while those at 15,000 Pa were identified for CFD validation purposes

Table 4 CFD model verification/validation matrix

Sample	Surface T (K)	Stagnation pressure (Pa)
CVD-SiC	1400	2000
CVD-SiC	1400	15,000
PM1000	1400	2000
PM1000	1400	15,000
CVD-SiC	1600	2000
CVD-SiC	1600	15,000
PM1000	1500	2000
PM1000	1500	15,000

Both nitrogen and air plasmas are rebuilt for each case. Cases with stagnation pressures of 2000 Pa are used to verify the CFD model, while cases at 15,000 Pa provide validation via model extrapolation

model extrapolates to the higher pressure conditions correctly without incorporation of the 15,000 Pa conditions in the model calibration. This behaviour is anticipated due to the physical basis of the model formulation. It is physical model parameters (which might also be directly determinable from other types of experiment or detailed physics simulations) that are being calibrated in the present case, rather than the coefficients (of a polynomial for example) used in a purely correlated approach, which are not strictly valid outside the functional parametric fitting range.

It was expected that EXPERT would fly during the course of this study, in which case the flight data would have been rebuilt to provide a final validation of the model. Flight data were not available; therefore, heat fluxes were calculated in a predictive capacity for comparison at such time the data are available. One point on the trajectory will be rebuilt close to peak catalycity. An important catalysis experiment on EXPERT is to measure the heat flux overshoot at the C/C-SiC/PM1000 junction; attention will be paid to this in the CFD computation. This region was identified as an important area for future investigation from early on in the EXPERT mission design.

3 Experimental campaign

The wide pressure range addressed within the experimental campaign has the drawback that the atomic species partial pressure is low for most of the experimental conditions. Therefore, the heat flux due to catalytic recombination is low in comparison with Fourier heating. In these cases, the signal to noise ratio was poor. Hence, recombination coefficients could not be determined for all experimental conditions.

3.1 PWK3 synthesis

From the initial facility calibration phase, it was determined that all twelve conditions are reproducible in PWK3, and that the flow characterisation could be accomplished, by assessing axial and radial profiles of the key plasma parameters. An enthalpy probe [13] (which employs calorimetric dependency of variable cold gas injection) and Pitot probe were used to characterise plasma freestream parameters. Flow velocity, concentration of atomic species, and temperature are derived from these diagnostics using thermal equilibrium assumptions. Characteristic plasma freestream conditions determined for each test condition are given in Table 5. Reconstruction of the PWK3 conditions with the URANUS CFD code is required for determination of the recombination coefficients.For both 100 and 500 Pa conditions in oxygen and nitrogen, the flow discharges are supersonic. For 2000 Pa conditions, the plasma discharge is subsonic. For nitrogen tests, a convergent conical nozzle has been used for a proper ignition of the plasma and for better plume stabilisation. The convergent nozzle throat diameter is 50 mm with a convergence angle of 30°. In all other tests, the plasma exits into the test chamber from the induction chamber which has a diameter of 83 mm.

From the main test campaign, it can be concluded that the PM1000 temperature records during the facility calibration phase and the main tests are similar to each other and within the measurement uncertainties, the main test campaign is a verification of the experimental calibration tests. On the other hand, for CVD-C/C-SiC, as the material was not available during the facility calibration phase, SiC material was used instead. The temperature records can, therefore, only be compared with the SiC records. The result of this comparison is that in all conditions except for the N_2 2000 Pa condition, the 1400 K for CVD-C/C-SiC

Table 5 Characteristic plasma freestream parameters determined for the PWK3 test conditions

Test condition	Test gas	x (mm)	P_{stag} (Pa)	u_∞ (m/s)	h_0 (MJ/kg)	T_∞ (K)	c_∞
CVD-SiC 100 Pa	O_2	228	166	2660	23.31	3310	0.996
PM1000 100 Pa	O_2	620	120	1790	15.55	2700	0.802
CVD-SiC 500 Pa	O_2	355	535	1880	14.39	2810	0.757
PM1000 500 Pa	O_2	535	480	1567	10.14	2650	0.509
CVD-SiC 2000 Pa	O_2	235	2110	374	9.63	2980	0.520
PM1000 2000 Pa	O_2	300	2070	230	5.35	2640	0.178
CVD-SiC 100 Pa	N_2	226	130	2526	27.84	4850	0.666
PM1000 100 Pa	N_2	364	85	1648	17.61	4570	0.419
CVD-SiC 500 Pa	N_2	430	550	2014	15.28	4680	0.287
PM1000 500 Pa	N_2	510	515	1706	10.44	4330	0.114
CVD-SiC 2000 Pa	N_2	370	2000	1080	11.74	4850	0.177
PM1000 2000 Pa	N_2	415	1995	736	7.03	4020	0.015

Distance from the nozzle exit x, freestream (inputs to recombination coefficient determination) velocity u_∞, temperature T_∞, and atomic mass fraction c_∞, measured stagnation pressure P_{stag} and total enthalpy h_0 are given

is obtained at shorter distances from the generator exit than the 1400 K for SiC. The high catalytic behaviour of PM1000 is in all conditions an issue. For most of the PWK3 operational configurations, a reduced electric power or a higher gas flow rate was required to minimise the enthalpy of the flow.

Surface analyses, such as material emissivity, are assessed in parallel with the emissivity measurement facility (EMF). Raw sample emissivity is used for setting pyrometers and thermocamera and has a certain controllability of the surface temperature during the test, while post-test emissivities are done to finally correct the obtained temperatures and to determine the radiative heat flux needed for the recombination coefficient determination methodology.

Existing methodologies to experimentally determine the recombination coefficients γ_i are based on heat flux measurements on material samples exposed to a dissociated flow. The reference method presented by Scott [19], and direct method from Pidan [18] and Massuti-Ballester [14], apply analytical solutions for the boundary layer problem following Goulards theory [7], to isolate from the total heat flux the part corresponding to the recombination of species at the surface. Strong assumptions in these methods, such as a frozen boundary layer, forced the introduction of more accurate non-equilibrium reconstructions of the boundary layer into the current methodology.

The improved methodology is based on an iterative approach where the flow reconstruction is corrected as the boundary layer accommodates to the final material catalysis. To assess this, the recombination coefficient obtained is implemented as a new gas–surface chemical model in URANUS and the flow reconstruction process is started again. In Fig. 1, a logic scheme of the methodology is presented.

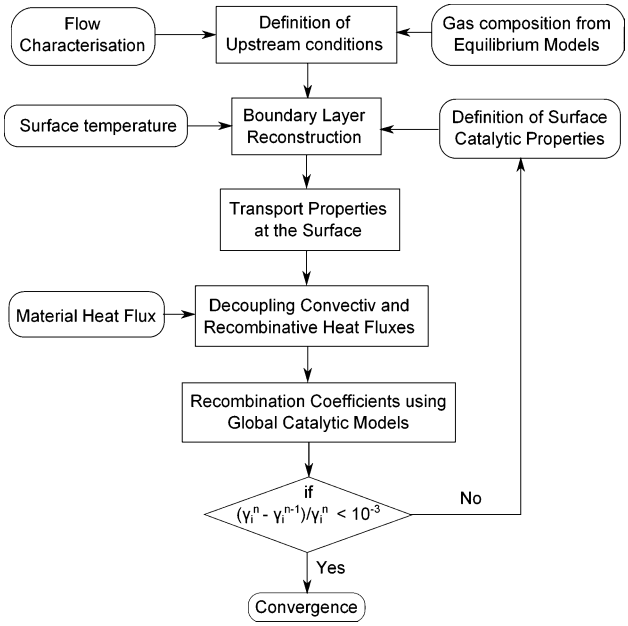

Fig. 1 Scheme of the new methodology for determination of recombination coefficients in PWK3

The old [18] and the new [14] methods use the same basic concept: separation of the total measured heat flux into two parts, one of which is used to infer the catalytic recombination coefficient of the material (the recombinative/diffusive heat flux), and another which has an indirect dependence on catalysis (the conductive/convective heat flux) is computed from the given conditions. Experimental techniques using this principle are designated as heat

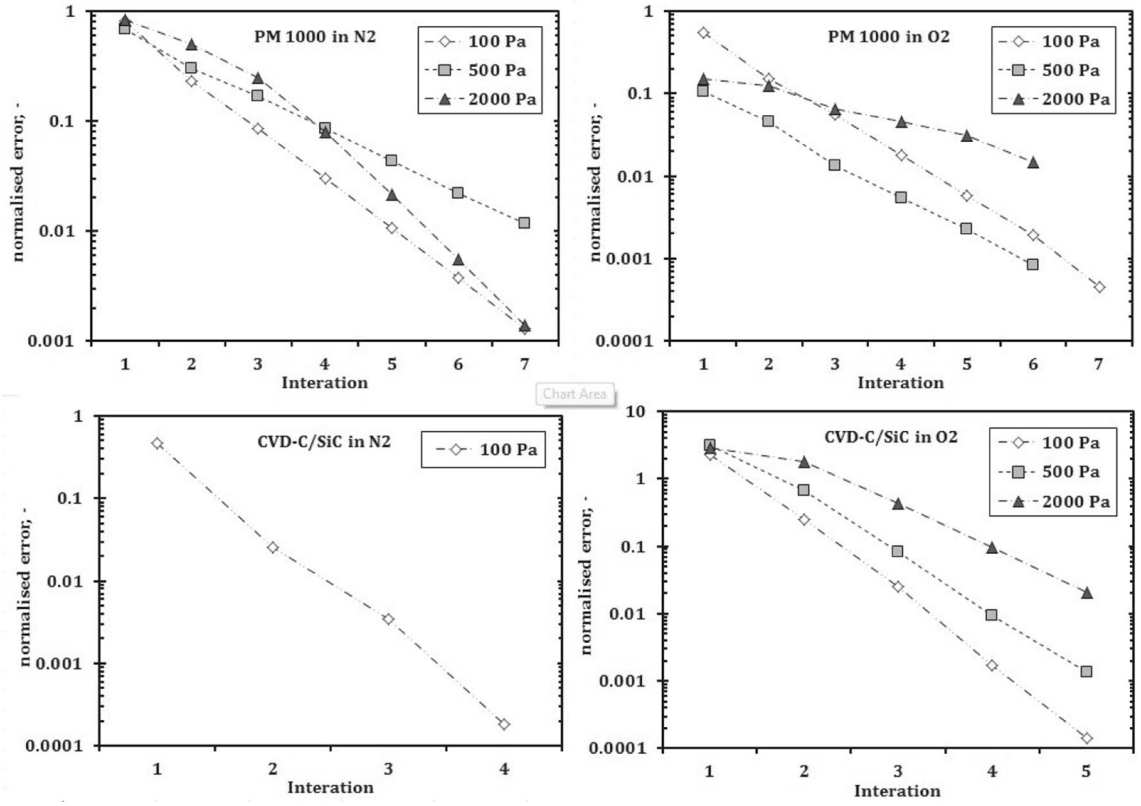

Fig. 2 Convergence of γ_i by rebuilding iterative times the boundary layer under new material catalycity

flux balance driven techniques. Significant variations in the determined recombination coefficients can occur from uncertainties in experimental enthalpy determination.

The Goulard theory applied in the old method assumes that the boundary layer is frozen and that the 'upstream conditions' (the flow between the bow shock and the boundary layer) are in thermal equilibrium. The new methodology lifts these restrictions, allowing a non-equilibrium flow reconstruction with the URANUS code. The equilibrium assumption for the upstream conditions has a significant effect to the results. However, the frozen boundary layer assumption has a higher impact. In a frozen boundary layer, the material catalycity has no influence on the boundary layer composition. Thus, the boundary layer has no concentration gradients, which cannot be the case because at the surface there are molecules continuously forming. Introduction of any non-equilibrium in the generated plasma flow from the nozzle can also be included in the improved methodology. This was not the case for the current work as further characterisation of the flow is required to establish the degree of non-equilibrium.

An iterative process is required because the catalycity of the material is coupled to the species concentration gradients through diffusive processes in the boundary layer. The conductive part of the heat flux is also dependent on the catalysis to some extent, due to variations in species stoichiometry at the surface. The flow reconstruction with URANUS is first performed with a random catalycity. Once the first iteration is fulfilled, the obtained recombination coefficient is then used for the next iteration of the boundary-layer flow reconstruction with URANUS. Repetition of this procedure adapts the boundary layer concentration gradients until convergence is obtained, i.e. the variation of recombination coefficients obtained between two iterations is small (<0.1 %). The recalculation process of the flow field is repeated several times until a converged value of the recombination coefficient is achieved. This convergence is shown for all conditions in Fig. 2. It was not possible to derive recombination coefficients on CVD-C/SiC in nitrogen flows for the 500 and 2000Pa conditions due to low degrees of molecular dissociation and the expected low catalytic efficiency.

A sensitivity analysis has been assessed by altering the mass specific enthalpy of the characterised flow ±20 %. The error bars shown in Fig. 3 represent the error propagation on the obtained recombination coefficients from an initial uncertainty of the aforementioned measurement technique of about ±20 %. The resulting γ_i are plotted in Fig. 3 over the partial pressure at the surface. Due to the different dissociation degrees on each condition and the material

catalycity influence on the final concentrations at the wall, the partial pressures obtained should not be mixed with the three target stagnation pressure of 100, 500 and 2000 Pa.

The results demonstrate a relationship between the $\ln(\gamma_i)$ and $\ln(P_i)$ for both materials and gases at least at respective temperature regimes. The methodology presented here has been contrasted with the reference method and the direct method by applying all three methods to the twelve experimental datasets.

Limited characterisation of the flow during the experimental campaign forced the use of equilibrium models for the estimation of the free flow composition and temperatures. Extended facility calibration and diagnostics should be fulfilled in future to improve the results and show the non-equilibrium behaviour of the plasma jet.

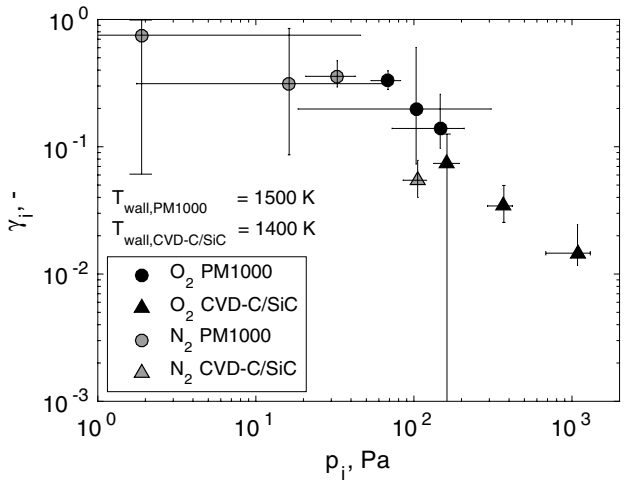

Fig. 3 γ_i over p_i for CVD-C/C-SiC and PM1000 for partially dissociated oxygen and nitrogen flows

Table 6 PWK3-derived recombination coefficients and atomic species partial pressures at stagnation for test conditions in oxygen and nitrogen plasmas

Test condition	Test gas	Recombination coefficient γ	Atomic partial pressure at the wall (Pa)
CVD-SiC 100Pa	O_2	0.069	160
CVD-SiC 500Pa	O_2	0.032	377
CVD-SiC 2000Pa	O_2	0.014	1083
PM1000 100Pa	O_2	0.337	66
PM1000 500Pa	O_2	0.144	148
PM1000 2000Pa	O_2	0.203	96
CVD-SiC 100Pa	N_2	0.050	104
PM1000 100Pa	N_2	0.353	31
PM1000 500Pa	N_2	0.312	17
PM1000 2000Pa	N_2	0.751	2.1

From the discussion on pressure dependencies of catalytic mechanisms in Sect. 2.1, it can be seen in Fig. 3 and Table 6 that only the LH mechanism is able to explain the observed trends in pressure. The nitrogen recombination coefficients on PM1000 (and more marginally the oxygen values on CVD-SiC) have sufficiently large uncertainties to infer a constant or increasing catalytic efficiency that might be explained by the ER mechanism. However, the data points of oxygen recombination on both PM1000 and CVD-SiC show the trend expected from low temperature behaviour of the LH mechanism. We are, therefore, led to conclude from the PWK3 synthesis that the dominant catalytic mechanism is Langmuir–Hinshelwood recombination in this regime. This does not exclude a relevant contribution from Eley–Rideal recombination to the total catalytic efficiency.

3.2 L2K synthesis

For L2K, three different pressure levels had been defined, i.e. 20, 50 and 200 hPa. The highest pressure level had to be reduced to 150 hPa to maintain a good optical view to the samples front surface which is required for reliable surface temperature measurements. The samples had a disk-like geometry, and were installed on the front surface of a cylindrical test assembly (see Fig. 4), in a geometrically identical fashion to the PWK3 test setup. For the facility calibration test campaign, the PM1000 samples were available, while the CVD-SiC samples had to be substituted by sintered SiC samples.

All facility calibration tests on the SiC samples could be completed in air as well as in nitrogen. For the tests at pressure levels of 20 and 50 hPa, a conical nozzle with an exit diameter of 100 mm was used. For a pressure level of 150 hPa, a shorter nozzle with an exit diameter of 50 mm had to be used. When performing the final validation tests on CVD-SiC samples, slight modifications to the identified operating conditions were necessary. With the PM1000 samples, the facility calibration tests could not be run as intended. During several tests, the ceramic SiC shell, which is needed for sample fixation, broke several times during testing, most probably due to differences in thermal expansion. Although a procedure was found to run selected tests, it was not possible to perform all calibration tests on PM1000 samples. From the tests that could be carried out, it was confirmed that the facility calibration was very close to the results obtained for SiC samples. Therefore, the remaining set of experimental calibration tests was run with SiC samples. Again, minor modifications to the identified operating conditions were necessary when running the final validation tests on PM1000 samples.

The validation test campaign was carried out with twelve samples of each material, i.e. CVD coated SiC and

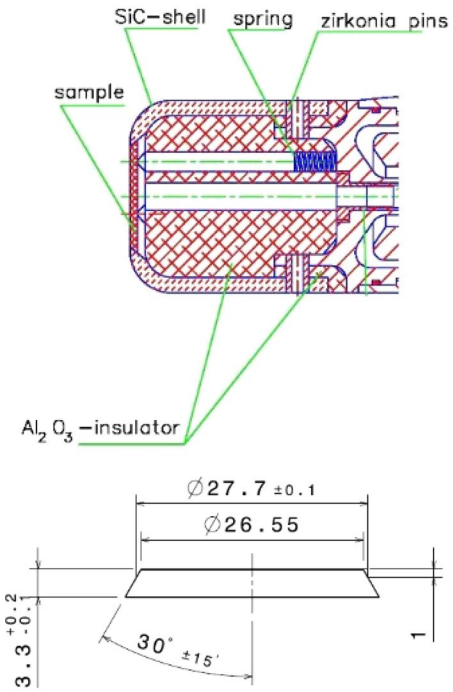

Fig. 4 Schematic of L2K test assembly and sample geometry (dimensions in mm)

PM1000. Due to the reason mentioned above, the operating conditions identified during facility calibration were not applied identically in the validation tests, but served as a good starting point for reaching the required test conditions. After thermal ageing of the SiC shell, the operational complications with the PM1000 samples did not reappear during the validation tests, and all tests were carried out nominally.

All specified tests conditions could be reached. During the tests, the sample's surface temperature was monitored with a pyrometer. Test conditions were adjusted until the specified surface temperatures, which had been appointed most important for numerical rebuilding and validation, were achieved with a deviation below ±10 K. Compliance to the pressure specification was considered more relaxed. Nevertheless, the pressure specifications of 20, 50, and 150 hPa were met within ±5 hPa. For pressure measurements, the sample was replaced by a standard Pitot probe.

For the L2K conditions, recombination coefficients were evaluated following Pidan's [18] extension to Goulard's method. An iterative procedure was applied with the methodology described in Fig. 1. Reconstruction steps were carried out with the TAU code. From the operational data, the facility's reservoir conditions were evaluated for all test conditions. It turned out that appreciable dissociation levels were achieved in the reservoir for air operation only, and in this case only for the lowest pressure level of 20 hPa and the highest temperatures levels, i.e. 1600 K on SiC and 1500 K on PM1000. For almost all other conditions, dissociation in the reservoir was found very low, in some cases negligible. For these conditions, the evaluation of recombination coefficients was found impossible for these test conditions, since the contribution of recombination to the surface heat flux was very small and the measured data could not be fit into the small span between the fully catalytic and non-catalytic cases.

Recombination coefficients could mainly be evaluated for the lowest stagnation pressure level of 20 hPa. In nitrogen flow, results were obtained for the high temperature cases only. For both materials, CVD-SiC and PM1000, a recombination of 0.02 was determined at 1600 and 1500 K, respectively. In air, results were obtained for both temperature levels. The recombination coefficients for oxygen and nitrogen are inseparable; an effective air recombination coefficient is, therefore, computed. However, at the gas temperatures found in the tests, it is not expected that there is a significant amount of dissociated nitrogen and the air recombination coefficients are assumed to be representative of oxygen. For both materials, the recombination coefficient decreases with increasing temperature at a pressure of 20 hPa. At 1400 K, the values are similar for both materials, 0.19 for CVD-SiC and 0.12 for PM1000. At the higher temperature condition, the recombination coefficient decreases by more than an order of magnitude for CVD-SiC, while the decrease is moderate for PM1000. At a pressure level of 50 hPa, only one recombination coefficient could be computed. For CVD-SiC at 1600 K, the value of γ is in the order of magnitude as found at 1400 K. Recombination coefficients that could be acquired from the L2K test campaign are summarised in Table 7. Characteristic plasma freestream conditions determined for each corresponding test condition are given in Table 8.

It is acknowledged that the recombination coefficients obtained in L2K differ significantly from those obtained

Table 7 L2K-derived recombination coefficients and atomic species partial pressures at stagnation for test conditions in air and nitrogen plasmas

Test Condition	Test Gas	Recombination coefficient γ	Atomic partial pressure at the wall (Pa)
S 1600K 20hPa	Air	0.0049	753
S 1400K 20hPa	Air	0.19	173
S 1600K 50hPa	Air	0.0015	986
S 1600K 20hPa	N_2	0.02	124
P 1500K 20hPa	Air	0.08	349
P 1400K 20hPa	Air	0.12	201
P 1500K 20hPa	N_2	0.02	33

Air recombination coefficients are computed as a 'total-effective' value; however, due to very low nitrogen dissociation, they may be considered as primarily oxygen recombination coefficients. Test material identification is abbreviated to P and S for PM1000 and CVD-SiC, respectively

Table 8 Characteristic plasma freestream parameters determined for the L2K test conditions for which recombination coefficients were derived

Test condition	Test gas	x (mm)	P_{stag} (Pa)	u_∞ (m/s)	h_0 (MJ/kg)	T_∞ (K)	c_∞
S 1600K 20hPa	Air	380	2510	3063	8.8	400	0.211
S 1400K 20hPa	Air	380	2100	2516	4.8	345	0.047
S 1600K 50hPa	Air	120	5330	2653	6.5	595	0.115
S 1600K 20hPa	N_2	380	2480	3208	7.5	546	0.026
P 1500K 20hPa	Air	380	2250	2674	6.0	361	0.096
P 1400K 20hPa	Air	380	2180	2540	5.0	348	0.055
P 1500K 20hPa	N_2	380	2360	3005	6.1	495	0.007

Distance from the nozzle exit x, freestream (inputs to recombination coefficient determination) velocity u_∞, temperature T_∞ and atomic mass fraction c_∞, measured stagnation pressure P_{stag} and total enthalpy h_0 are given.Test material identification is abbreviated to P and S for PM1000 and CVD-SiC, respectively

in PWK3 for equivalent nominal conditions. Uncertainties in the determination of heat flux using pyrometry are independent of the flow condition, which means that for the case of low dissociation, where small variations of heat flux are to be expected between fully and non catalytic scenarios, these inaccuracies (<10 % of the total heat flux) can be larger than the investigated catalytic part of the heat flux. This was more tolerable for the low dissociation level at PWK3, particularly with the improved data reduction methodology, but has a stronger impact for L2K-derived results. It should, therefore, also be considered that the cross facility comparison compares not only facility plasma flow conditions, but also the method used to obtain the recombination coefficients. The differences may also reinforce the complex pressure dependencies expected from heterogenous catalytic recombination. PWK3 tests show an increase of catalytic efficiency by lowering the partial pressure; it does not necessarily follow that this will be the case in other pressure regimes. It can happen that for a further reduction of the partial pressure the catalycity falls again. This behaviour has been observed on a copper oxide surface under the similar plasma conditions [15].

4 Numerical campaign

4.1 CFD model calibration

The model calibration had to distinguish between the two materials under investigation, namely PM1000 and CVD-SiC. Since parameter sets for catalysis modelling on SiC have already been published in the past [4, 6], the CVD-SiC model calibration will be explained first. As a first step, published recombination coefficients [16, 20, 21] together with the new measurements (Sect. 3) have been compared with the current model calibration [6]. Isobars of oxygen and nitrogen recombination coefficients are shown in Figs. 5 and 6, respectively. The broken lines show surface partial pressure isobars corresponding to the experimental points. The solid lines show surface partial pressure isobars at 1, 10,100,1000, 10,000 and 100,000 Pa as a reference. However, if the experimental conditions were close, the solid black lines were skipped.

As can be seen from Fig. 5, the old recombination data [20, 21] are represented quite well by the model calibration. Significant discrepancies can be observed when comparing the curves at 160 Pa (dashed), 377 Pa (dotted) and 1083 Pa (dash-dotted) in oxygen partial pressure with the measured points at these pressures. As can be seen, the recombination probability at these partial pressures is significantly overestimated and the maximum in recombination probability is shifted towards lower temperature. However, in [6] it was already stated that the partial pressure of the experiments in [20, 21] had to be assumed for the old model calibration. This offers a degree of flexibility to refit these data assuming a different atomic partial pressure, within the constraint of known total surface (stagnation) pressure.

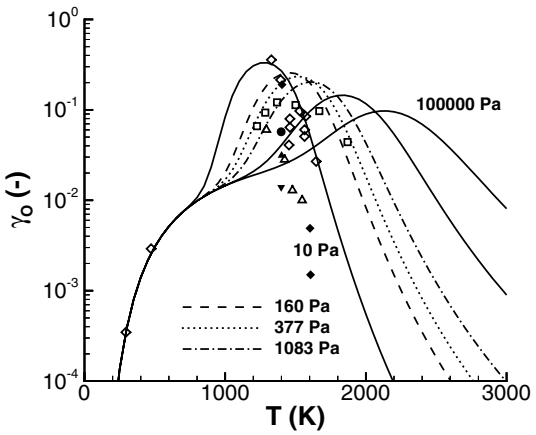

Fig. 5 Temperature and pressure dependency of the CVD-SiC oxygen recombination coefficient with old model calibration data [6] in comparison to the literature data (*empty diamond* [20], *empty triangle* [21], *empty box* [16]) and current measurements from L2K (*filled diamond*) and from PWK3 at 160 Pa (*filled circle*), 377 Pa (*filled triangle*) and 1060 Pa (*filled inverted triangle*) of oxygen partial pressures

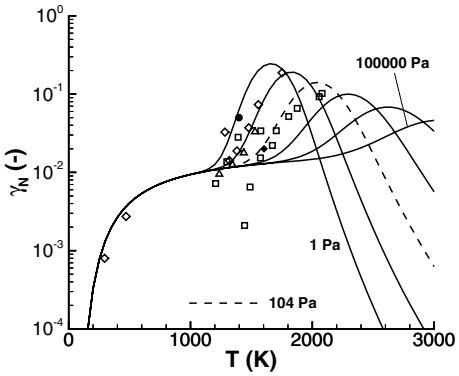

Fig. 6 Temperature and pressure dependency of the CVD-SiC nitrogen recombination coefficient with old model calibration data [6] in comparison to the literature data (*empty diamond* [20], *empty triangle* [21], *empty box* [16]) and current measurements from L2K (*filled diamond*) and from PWK3 at 104 Pa (*filled circle*) of nitrogen partial pressure

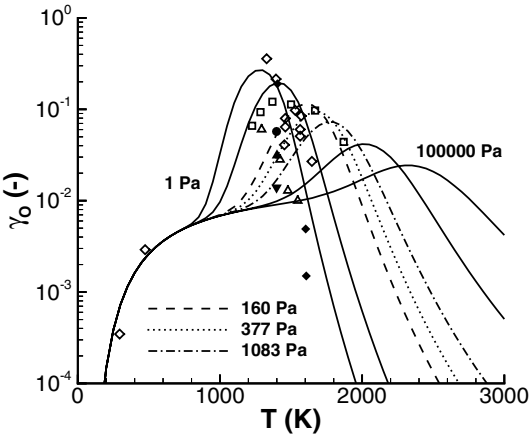

Fig. 7 Temperature and pressure dependency of the CVD-SiC oxygen recombination coefficient with new model calibration data in comparison to the literature data (*empty diamond* [20], *empty triangle* [21], *empty box* [16]) and current measurements from L2K (*filled diamond*) and from PWK3 at 160 Pa (*filled circle*), 377 Pa (*filled triangle*) and 1083 Pa (*filled inverted triangle*) of oxygen partial pressures

A similar observation as for oxygen recombination can be made for the nitrogen recombination shown in Fig. 6. However, in the nitrogen case the recombination coefficient at 104Pa in nitrogen partial pressure is significantly underestimated. Here, the recombination coefficient maximum is shifted towards higher temperature.

A manual fitting procedure is employed to recalibrate the model, in an attempt to provide model parameters that well represent their expected physical values. Further, not all of the model parameters can be determined independent of each other (the characteristic temperatures and the desorption energies in particular are strongly linked). Automatic fitting routines are not well suited in this respect. The PWK3-measured recombination coefficients are used to anchor the calibrations, with the L2K recombination coefficients, pre-existing PWK3 data [16], and old calibration data [20, 21] providing supplementary fitting data. From the experiments performed in Sect. 3, it is known that higher partial pressure to total pressure fraction improves the signal to noise ratio considerably. Hence, it might be expected that the partial pressures of the old data points are significantly higher than assumed for the previous calibration.

To account for the new measurements for oxygen, the characteristic temperature for surface diffusion was reduced to $\Theta_{\mathrm{Diff,O}} = 0.47992$ K (4.7992 K), where the previous value is given in braces. The activation energies for desorption and diffusion were increased to $D_{\mathrm{Des,O}} = 255$ kJ/mole (230 kJ/mole) and $D_{\mathrm{Des,O}} = 155$ kJ/mole (140 kJ/mole). To reduce the recombination coefficient at 1500 K while still reproducing the low temperature behaviour, the Eley–Rideal reaction parameters were set to $c_{\mathrm{ER,O}} = 0.009$ (0.035) and $A_{\mathrm{ER,O}} = 8$ kJ/mole (13kJ/mole). The model results with the updated parameter set are plotted in Fig. 7.

With exception of a measurement point at 1330K from Stewart [20], all other data points can be reproduced with the new data set. Especially, the new measurements can be reproduced very well. The L2K data points have actually been derived in air. However, due to the negligible nitrogen dissociation at the temperatures under investigation, it was assumed that the air recombination coefficients actually coincide with the oxygen recombination coefficients. The measurements from L2K at 1600 K are in a temperature regime where the recombination coefficient decreases with increasing temperature. Since the stagnation pressure for these measurements was high, a low dissociation degree and, therefore, a low oxygen partial pressure were expected. The data points correspond to model results at an oxygen partial pressure below 1 Pa. Surprisingly, the data point at 1400 K where an even lower oxygen partial pressure is expected corresponds to the model results in the pressure range 1–10 Pa. As the ER-mechanism is independent of pressure at low temperature, the ER-mechanism is not able to rebuild the pressure dependency. The final calibrated model data for all recombination coefficients are collected in Table 9.

During the study, the PWK3 nitrogen conditions had been confused. Therefore, an improper nitrogen recombination calibration was published in [3]. The measurements of nitrogen recombination on CVD-SiC provided only two data points: one from PWK3 at 104Pa of nitrogen partial pressure and another from L2K. Especially the data point from PWK3 allows due to the combination of recombination probability with partial pressure for a significantly better grading of the available data from the literature. To reproduce the new PWK3 data

point, the activation energies for desorption and diffusion were reduced to $D_{Des,N} = 290\,\mathrm{kJ/mole}$ (340 kJ/mole) and $D_{\mathrm{Diff,N}} = 187\,\mathrm{kJ/mole}$ (240 kJ/mole). To reduce the recombination coefficient at 1235 K while still reproducing the low temperature behaviour, the Eley–Rideal reaction parameters were set to $c_{\mathrm{ER,N}} = 0.007$ (0.011) and $A_{\mathrm{ER,N}} = 7$ kJ/mole (8 kJ/mole). With this calibration, the new data point which is marked in green in Fig. 8 can be reproduced very well. However, one data point from [14] at 1444 K cannot be reproduced.

Due to the previous lack of experimental data, no calibrated reaction model coefficient data set for PM1000 was initially available. Within the experimental campaign conducted for this study, six new data points have been provided by IRS (PWK3 facility; see Sect. 3.1) and three by DLR-K (L2K facility; see Sect. 3.2). The data points from PWK3 and L2K are marked by the filled symbols in Figs. 9 and 10. The PWK3 oxygen data points have been obtained at 66 Pa (filled circle), 96 Pa (filled triangle) and 148 Pa (filled inverted triangle) of atomic oxygen partial pressure. They are shown together with data from the literature which is marked by open symbols, the data points from L2K (filled diamond) and the calibration curves of the model (dashed 66 Pa, dotted 96 Pa and dashed-dotted 148 Pa) in Fig. 9. The nitrogen results have been determined at 2Pa (filled inverted triangle), 17Pa (filled triangle) and 31Pa (filled circle) of atomic nitrogen partial pressure. They are shown together with data from the literature, the data point from L2K (filled diamond) and the calibration curves of the model (dashed: 2 Pa, dotted: 17 Pa and dashed-dotted: 31 Pa) in Fig. 10. For the reproduction of the experimental data on PM1000, it was necessary to conclude from the low temperature data of Stewart [22] (empty diamond) that the ER mechanism is independent of temperature. Therefore, the Eley–Rideal constants were set to $c_{ER,O} = 0.0015$, $c_{ER,N} = 0.0067$ and $A_{ER} = 0$ kJ/mole. As the recombination probabilities on PM1000 come close to unity, the adsorption probability must be close to unity as well. Hence, $\tilde{n}\pi\sigma^2_{Ad,O} = 0.9$ and $\tilde{n}\pi\sigma^2_{Ad,N} = 1.0$ were set. Steward obtained the recombination coefficients in a side-arm reactor at 35Pa of total pressure. It is assumed that the atomic species mole fraction in these experiments was ranging between 1 and 100 %. Therefore, during the model calibration it was requested that Stewart's data points should be bound by an atom partial pressure range from 0.35 to 35 Pa. Model calibration curves at 0.35, 3.5 and 35 Pa of atom partial pressure are shown by dashed double-dotted lines in Figs. 9 and 10. The increase in recombination coefficients with temperature below 1600 K gives rise to the activation energies $A_{LH,eff,OO} = D_{Diff,O} = 65$ kJ/mole and $A_{LH,eff,NN} = D_{\mathrm{Diff,N}} = 68$ kJ/mole. It is noted that the LH activation energy of oxygen is in reasonable agreement with the fitted value of 51 kJ/mol from catalytic air recombination data produced at similar enthalpy and pressure (1500

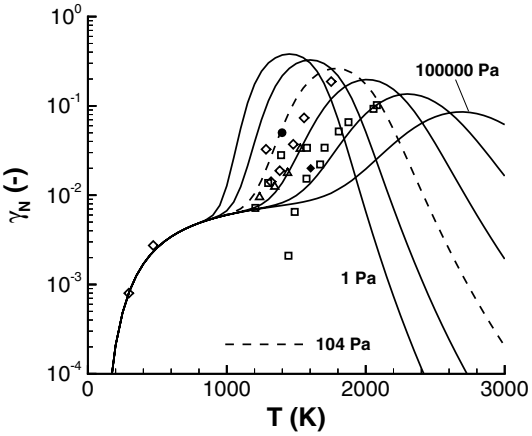

Fig. 8 Temperature and pressure dependency of the CVD-SiC nitrogen recombination coefficient with new model calibration data in comparison to the literature data (*empty diamond* [20], *empty triangle* [21], *empty box* [16]) and current TRP measurements from L2K (*filled diamond*) and from PWK3 at 104 Pa (*filled circle*) of nitrogen partial pressure

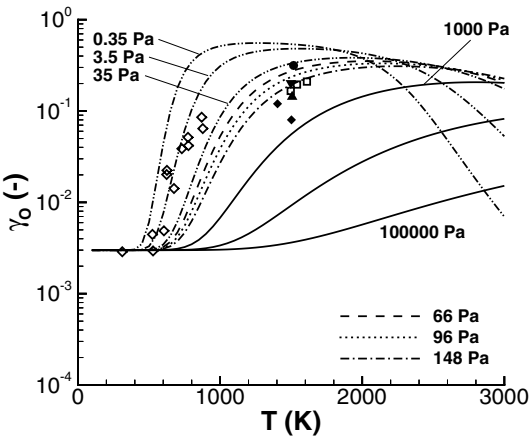

Fig. 9 Temperature and pressure dependency of the PM1000 oxygen recombination coefficient with new model calibration data in comparison to the literature data (*empty box* [16], *empty diamond* [22]) and current TRP measurements *filled diamond* L2K, *filled circle* PWK3 at 66 Pa, *filled triangle* 96 Pa and *filled inverted triangle* 148 Pa of oxygen partial pressure

Pa of stagnation pressure) by Panerai et al. [17]. These data are assumed representative of oxygen due to low levels of dissociation evaluated at the surface. At higher pressures (7500 and 10,000 Pa stagnation pressure), a fit of 20 kJ/mol is obtained. It is also noted that the recombination coefficients reported by Panerai et al. are notably lower than those measured in the current work, particularly at high pressure. Uncertainty margins are not given on the recombination coefficient by Panerai et al.; however, as shown by our own experience, they can be significant and, therefore, differences at 15,000 Pa may be reconciled with further investigation. A

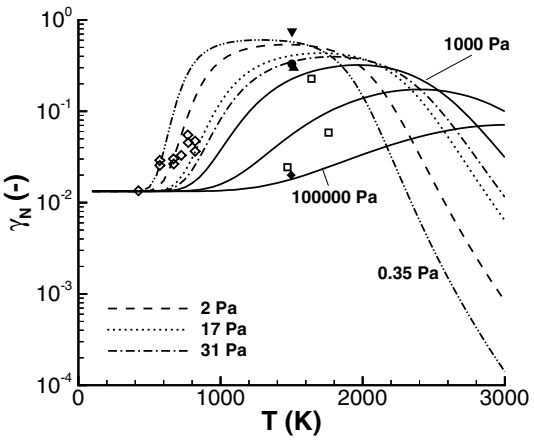

Fig. 10 Temperature and pressure dependency of the PM1000 nitrogen recombination coefficient with new model calibration data in comparison to the literature data (*empty box* [16], *empty diamond* [22]) and current measurements *filled diamond* uses of phenolic resin L2K, *filled circle* PWK3 at 31 Pa, *filled triangle* the data points from 17 Pa and filled inverted 2 Pa of nitrogen partial pressure

Table 9 Reaction coefficients for the recombination of nitrogen and oxygen on PM1000 and CVD-SiC

Material	PM1000		CVD-SiC	
Adsorbens	N	O	N	O
$\tilde{n}_0\,(m^{-2})$	10^{15}	10^{15}	10^{19}	10^{19}
Θ_{Diff} (K)	4.7992	4.7992	4.7992	0.47992
Θ_{Des} (K)	47992	479.92	1589.4	1714.0
D_{Diff} (kJ/mole)	68	65	187	155
D_{Des} (kJ/mole)	200	200	290	255
A_{Ad} (kJ/mole)	0	0	0	0
$A_{Ad,max}$ (kJ/mole)	20	20	29	25.5
$\tilde{n}_0\pi\sigma_{Ad}^2(-)$	1.0	0.9	0.7	0.7
c_{ER} (-)	0.0067	0.0015	0.007	0.009
A_{ER} (kJ/mole)	0	0	7	8
c_{LH} (-)	34.6	34.6	345998	345998
A_{LH} (kJ/mole)	68	65	194	163

significant drop in recombination coefficient at higher pressure is supported by the model calibration in Fig. 9. The publication of Panerai et al. was not known to us at the time of conducting the work presented here, but it could be used in the future to improve the PM1000 model calibration, given the limited number of data points available here with known partial pressure.

The final choices for the remaining model parameters are highly questionable. Desorption energies were set to $D_{\mathrm{Des,O}} = D_{\mathrm{Des,N}} = 200$ kJ/mole. However, desorption energy mainly affects the high temperature behaviour of the catalysis model, i.e. at temperatures above the melting point of PM1000. More problematic is the specification of the characteristic temperatures for the vibration tangential and perpendicular to the surface and the active site number density. All of them are strongly coupled such that changes in one parameter require compensation by the other two. Employing an attempt frequency of $10^{-15}\mathrm{s}^{-1}$ [10] would result in a characteristic temperature of 47992K. Using this value would require an active site number density of $10^{13}\mathrm{m}^{-2}$ in case of oxygen recombination which results in combination with the reactive area in a reactive cross section of $1.7 \times 10^{-7}\mathrm{m}^2$ per active site. As this was considered far too large, the active site number density was set to $\tilde{n}_0 = 10^{15}\mathrm{m}^{-2}$. To cover the experiments, the characteristic temperatures were then set to $\Theta_{\mathrm{Des,O}} = 479.92\mathrm{K}$, $\Theta_{\mathrm{Diff,O}} = 4.7992\mathrm{K}$, $\Theta_{\mathrm{Des,N}} = 47992\mathrm{K}$ and $\Theta_{\mathrm{Diff,N}} = 4.7992\mathrm{K}$.

As mentioned above, all model parameters derived from this work are summarised in Table 9.

4.2 CFD comparison campaign

The L2K supersonic nozzle and stagnated test-sample flowfields were rebuilt for each of the conditions of the CFD test matrix (Table 4) using both TINA and TAU. Additional 5000Pa cases were also rebuilt with TAU. It is evident from previous discussion of the L2K synthesis (Sect. 3.2) that the final high pressure validation data was not produced due to low degrees of molecular dissociation. Therefore, strictly only a verification and consolidation of the catalytic behaviour observed in the tests could be provided by the CFD model. For reasons of brevity, the exact details of the extensive CFD test-rebuilding campaign are omitted in favour of a general overview of the findings.

CFD rebuilds of the L2K tests were performed using the facility supplied mass flow rates, nozzle-reservoir conditions for pressure and enthalpy, and test-chamber ambient pressure. The measured emissivity (from comparisons of two-colour and spectral pyrometer measurements) was used as an input to a radiative equilibrium model boundary condition. The in-depth conductive losses from the sample surface energy balance were also incorporated using thermal analyses conducted in the recombination coefficient derivation phase of the experimental campaign. CFD computed stagnation pressure and wall temperature (or the corresponding heatflux) were compared against the experimentally acquired measurements.

In general, it was not possible to bound any of the high stagnation pressure (15,000 Pa) L2K test case measurements of surface temperature within the limits of any possible catalytic heating effect (the non-catalytic to fully catalytic range). A number of low stagnation pressure cases were seen to be bound by the catalytic limits of heat-flux and, in general, the performance of the partial catalytic model for these cases was favourable, providing a

Table 10 Comparison of rebuilt TINA CFD stagnation pressure and wall temperature with experimentally measured values from the L2K validation campaign. CFD computed non-catalytic (nc), fully catalytic (fc) and partially catalytic (pc) wall temperatures are given. Test material identification is abbreviated to P and S for PM1000 and CVD-SiC, respectively

Test condition	Test gas	L2K P_{stag} (hPa)	CFD P_{stag} (hPa)	L2K T_w (K)	CFD $T_{w,nc}$ (K)	CFD $T_{w,fc}$ (K)	CFD $T_{w,pc}$ (K)
S 1400 K, 20 hPa	Air	21.0	19.7	1404	1290	1381	-
S 1600 K, 20 hPa	Air	25.1	21.7	1603	1530	1789	1694
P 1400 K, 20 hPa	Air	21.8	20.0	1404	1310	1413	1411
P 1500 K, 20 hPa	Air	22.5	20.4	1502	1358	1516	1513
S 1400 K, 150 hPa	Air	152	157	1399	1537	1549	-
S 1600 K, 150 hPa	Air	147	153	1610	1669	1735	-
P 1400 K, 150 hPa	Air	150	157	1403	1590	1605	-
P 1500 K, 150 hPa	Air	147	155	1504	1627	1658	-
S 1400 K, 20 hPa	N_2	24.0	22.4	1403	1400	1402	-
S 1600 K, 20 hPa	N_2	24.8	23.0	1604	1573	1657	1602
P 1400 K, 20 hPa	N_2	24.0	22.1	1393	1378	1380	-
P 1500 K, 20 hPa	N_2	23.6	22.1	1497	1493	1518	1509
S 1400 K, 150 hPa	N_2	155	171	1405	1569	-	-
S 1600 K, 150 hPa	N_2	153	168	1606	1754	1754	-
P 1400 K, 150 hPa	N_2	155	169	1399	1526	-	-
P 1500 K, 150 hPa	N_2	156	169	1503	1678	1678	-

verification of the calibrated catalytic CFD model. A number of TINA computed stagnation conditions are compared against experimental measurements in Table 10. The partial catalytic model results are given where the experimentally measured temperature was bound by the non-catalytic and fully catalytic CFD rebuilds. The fully catalytic computation was omitted from the CFD campaign in a number of cases where it was evident that the experimental test could not be rebuilt for the aforementioned reason.

A considerable effort was made to try and numerically bound the measured surface-temperature/heatflux of the high pressure cases (or match it where there was no appreciable difference between non-catalytic and fully catalytic cases) during the CFD campaign unsuccessfully. We are led to conclude that the catalytic range was too small (due to low facility dissociation degrees) within the limitations of the experimental accuracy and of the overall CFD model (not just the catalytic model boundary condition). The accurate computational characterisation of flow-fields in plasma wind tunnels is very challenging and relies on equilibrium assumptions in the reservoir. This topic alone is the subject of much ongoing research in the aerothermodynamics community. While the improved assessment of the low pressure L2K conditions provides verification, the intended extrapolation to high pressure remains incomplete for the SiC and PM1000 model calibrations determined in Sect. 4.1.

The numerical campaign supports the findings of the experimental campaign, albeit with the trivial assertion of limited potential for catalytic influence. The absence of a final model validation is neither a shortcoming of the modelling nor experimental measurements, since there was barely any oxygen dissociation at the 15,000 Pa conditions. It was, therefore, impossible to determine a recombination coefficient. The verification rebuilds at 2000Pa (with higher enthalpy) were on the whole successful (this should be expected because a recombination coefficient could be extracted). The risk of the enthalpy, being too low, was realised at the outset of the study, but was deemed acceptable to acquire the temperature ranges pertinent to the EXPERT material interface. The validation strategy as a whole is considered successful, given that all other goals of the study were achieved and, in principle, an extension of the work to use higher enthalpy flows could provide the required model validation data.

The CFD model has been applied previously [5] (with a silica calibration) using equivalent hyperboloids representative of STS-2 to rebuild flight center-line heatflux data [23, 24]. This validation was repeated under the framework of the current study and a cross-code verification was, therefore, obtained. A comparison of catalytic models computed with the TINA code at 66.81 km ($\rho = 1.216 \times 10^{-4} kg/m^3$, $T = 230K$, $v = 6.05km/s$) is given as an example in Fig. 11. The model described in Sect. 2.1 is able to closely represent the STS-2 flight data at surface pressures in this instance in the region ~4200–2500 Pa. Other trajectory points have also been considered with a similar outcome.

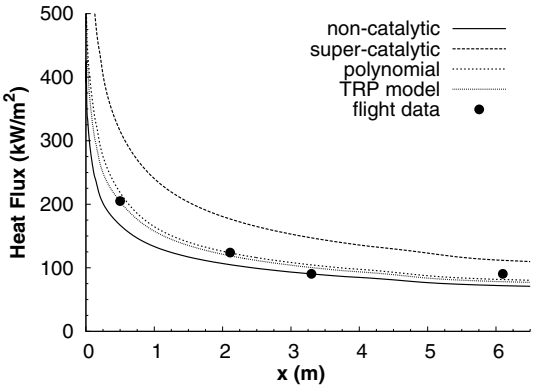

Fig. 11 Comparison of TINA CFD heatflux predictions with various catalytic models for STS-2 at 66.81 km. The model closely matches the performance of a temperature-dependant polynomial fit [5] to catalytic recombination data of silica

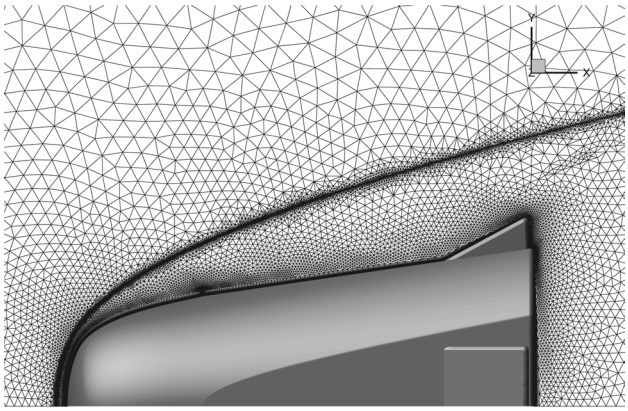

Fig. 12 Cut through the hybrid 3D grid employed for the simulation of the flow around EXPERT

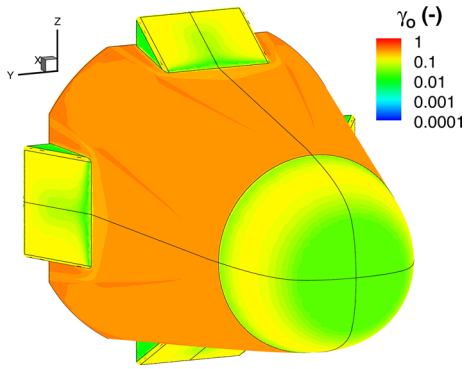

Fig. 13 Distribution of the oxygen recombination coefficient on EXPERT. The nose and the flaps were computed employing the current CVD-SiC catalysis model. The remaining parts are computed employing the PM1000 catalysis model

In the STS-2 flight case, the model parameters were evaluated from physical model constants inferred or measured from other works, and in come cases calibrated to match available recombination coefficient data [5]. In many cases, the partial pressures of the atomic species were either not known (and were estimated) or the pressure range was narrow. In Fig. 11, it is seen that the catalytic model computation is comparable to a correlated function of temperature only. This is to be expected given the narrow range of pressures covered and the use of the same fitting data. A concern of this previous application of the CFD model (and motivation for the current model validation philosophy) was that on a different trajectory profile (with different pressure ranges) the correlation may not perform as well due to a lack of pressure dependence and the model could have significant uncertainty due to a narrow spread of experimental pressures used to calibrate it.

In the current work, a pressure dependence of catalytic recombination has been demonstrated, and the model has been calibrated against test data at a wide range of known pressures. Concerns of the previous STS-2 model validation have, therefore, been addressed for CVD-SiC and PM1000 model calibrations. The model validation status is, therefore, considerably improved upon for this EXPERT oriented model compared with the STS-2 model application.

4.3 EXPERT

The new models were applied to the trajectory point at 50km of altitude on the EXPERT vehicle. At this altitude, the flow is characterised by $T = 270.06K$, $\rho = 1.04419 \times 10^{-3} kg/m^3$ and $v = 4976.1$ m/s. For the determination of the surface temperature, a radiation equilibrium surface was assumed employing the emissivities 0.63 and 0.73, determined in the L2K facility for PM1000 and CVD-SiC, respectively.

4.3.1 3D simulation

The 3D flow was simulated with TAU employing a hybrid, eight times adapted grid with 9.5 million grid points. The boundary layer is resolved with 45 structured grid layers. The normal resolution at the surface is 3×10^{-7}m. The surface itself is discretized by 77221 grid points. A cut through the *xy*-plane of the final grid is shown in Fig. 12. Figure 13 shows the distribution of the oxygen recombination coefficient on the EXPERT surface. The nose and the flaps were simulated employing the CVD-SiC catalysis model. At all other parts of the surface, the PM1000 model was applied. The PM1000 recombination coefficient is roughly one order of magnitude higher than the CVD-SiC recombination coefficient.

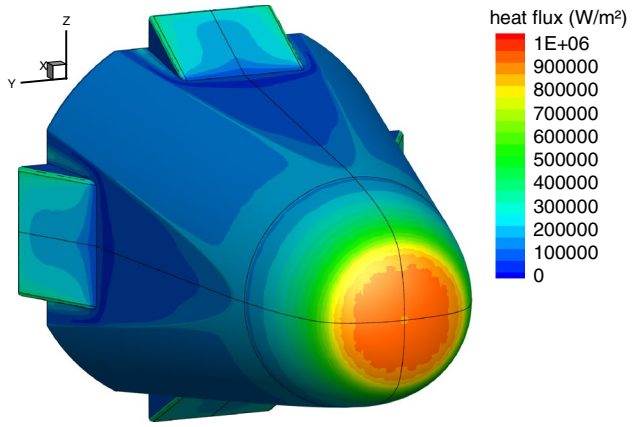

Fig. 14 Heat flux distribution on EXPERT employing the current CVD-SiC and PM1000 catalysis models

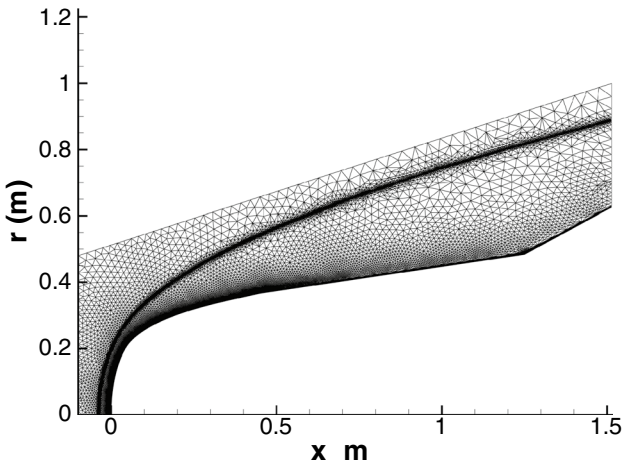

Fig. 15 Axisymmetric grid for the simulation of the flow-field around EXPERT

Fig. 14 shows the corresponding surface heat flux distribution. Due to the significantly higher recombination coefficient on PM1000, an abrupt increase in surface heat flux can be observed at the junction between CVD-SiC and PM1000 at $x = 0.4$ m where the CVD-SiC nose cap ends. An abrupt decrease of the surface heat flux can be observed at the PM1000/CVD-SiC junction at the flaps. Since the temperature at flap roots is only about 1000K, this is not critical for the TPS design.

4.3.2 Axisymmetric simulations

Since three-dimensional simulations are rather time consuming, the influence of different catalysis models was investigated based on axisymmetric simulations. The axisymmetric simulation makes use of the vehicle contour in the *xy*-plane. The final axisymmetric grid is shown in Fig. 15.

The hybrid axisymmetric grid resolves the boundary layer with 45 structured rectangular cells. The surface normal resolution is 3×10^{-7}m as for the 3D simulation. The final grid obtained after eight adaptation steps consists of 38224 grid points and resolves the surface with 510 points. In Fig. 16, the temperature distribution of the axisymmetric simulation (dashed line) is shown along the x-axis of EXPERT in comparison with the 3D temperature distribution (solid line) in the *xy*-plane. Very good agreement of the temperatures can be observed for $x < 0.2$ m. Slight discrepancies are visible rearwards up to $x < 0.5$ m. However, the temperature difference at the junction between PM1000 and CVD-SiC ($x = 0.4$ m) is nearly identical when comparing the axisymmetric with the 3D result. The 3D and the axisymmetric simulations show a temperature difference of $\Delta T_{3D} = 1539\text{K} - 1371\text{K} = 168\text{K}$ and $\Delta T_{Axi} = 1578\text{K} - 1431\text{K} = 147\text{K}$, respectively. For $x > 0.5$ m significant temperature, differences arise since 3D effects become important.

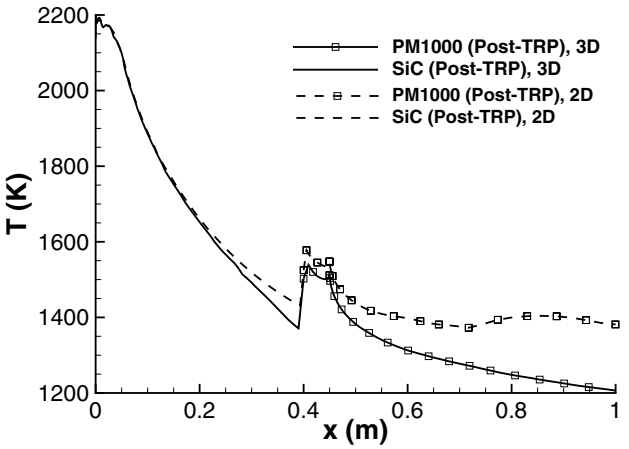

Fig. 16 Comparison of 3D with axisymmetric (2D) surface temperature distributions along the *x*-axis of EXPERT

In Fig. 17, the radiation equilibrium surface temperatures for different surface catalysis model assumptions are compared.

The dotted line marks the worst case where CVD-SiC is considered non-catalytic and PM1000 fully catalytic. The actual heat shield design is based on this conservative assumption [2]. As can be seen, the temperature of the PM1000 at the junction exceeds 2000 K. The dashed line shows the status of the catalysis model parameters prior to this TRP. Here, the model parameters given in [6] were used for CVD-SiC and PM1000 was assumed fully catalytic. With this setting, the PM1000 temperature at the junction becomes 1591 K. The solid line marks the result obtained with the new model parameters given in Table 9. Although the recombination coefficient on PM1000 is significantly below unity, the computed

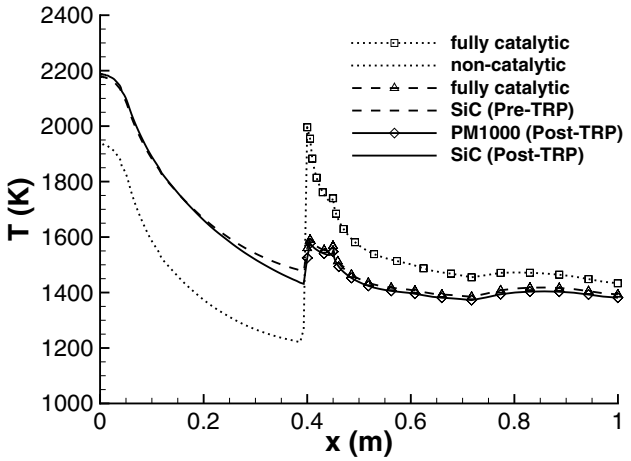

Fig. 17 Axisymmetric surface temperature distributions employing different catalysis models for CVD-SiC and PM1000

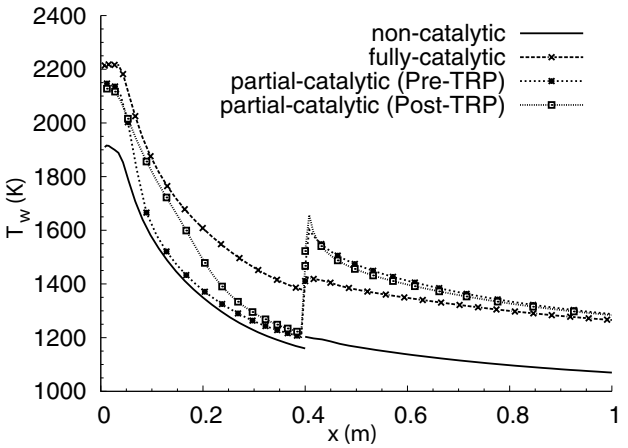

Fig. 18 Comparison of radiative equilibrium surface temperatures along the EXPERT fore-body at 50 km of altitude, obtained with varying catalytic models in TINA

temperature at the junction is 1578 K, which is only slightly lower than the previous result with fully catalytic surface assumption.

Similar observations can be made with the TINA implementation (Fig. 18). Note that the TINA axisymmetric body is based on the body shape in between the flaps. The non-catalytic, fully catalytic and TRP models with both the pre-TRP and post-TRP calibrations of CVD-SiC and PM1000 are compared. The temperature at the junction is of primary interest, where it is found in TINA that the post-TRP calibration increases the peak temperature from 1602 to 1657 K. While this is not large, compared with the range of radiative equilibrium temperatures encountered on the vehicle, this is significantly closer to the PM1000 melt temperature (∼1680 K). Modelling differences between the two codes exist, which prevent exact quantitative agreement. In particular, a difference in transport models (for which there is a dependency of the catalytic recombination coefficient) exists.

Despite numerical differences, the computations with both TAU and TINA confirm that the EXPERT conservative design is justified even with consideration of this more advanced model.

5 Conclusion

The priorities identified at the outset (Sect. 2) were successfully addressed by the synthesis of this project. High-quality experimental measurements of nitrogen and oxygen recombination coefficients on LEO re-entry materials provide a new set of validation data at a range of stagnation pressures relevant to LEO. All the planned test conditions were met, but due to low dissociation levels there was some difficulty extracting the catalytic efficiency from the measurements. However, this has led to an improved, more robust, data reduction technique. An improved catalytic CFD model now exists for use on these materials. The pre-existing model calibration for CVD-SiC was improved to capture the new validation data and other data in the literature. A first model calibration for PM1000 was developed. While validation through extrapolation of the model to high pressure could not be performed, the improved calibration of the model gives increased confidence. This is increased further with the demonstration of consistencies throughout the project between the CFD codes TAU, TINA and URANUS.

The work presented here provides the first confirmation of the pressure dependency of catalytic recombination. The Langmuir–Hinshelwood mechanism is identified as the only mechanism that can give the observed trend in pressure. The consistency with experimental observation and model further enhances confidence in the CFD model. These increased confidences, along with experimental measurements on PM1000 close to the melting point, confirm the close proximity of radiative equilibrium temperatures to the melting point of PM1000 on the EXPERT nose-cone material junction.

The primary difficulty in executing the validation methodology was the low degree of dissociation found in the facilities. This was identified as a possible problem at the outset of this study; however, the low heatflux high pressure scenarios relevant to EXPERT were prioritised. This leads to low enthalpy and, therefore, low dissociation levels. The low dissociation levels led to difficulties in experimental data reduction and CFD rebuilding, as the heat-flux range spanned by non-catalytic and fully catalytic surface responses was too small compared with the variations caused by modelling assumptions and experimental uncertainties. The high pressure recombination coefficients

could, therefore, not be obtained and the calibrated CFD catalytic model validation could not be extrapolated beyond the trivial result, which confirms that there is no catalytic effect for these arc-heater conditions.

Despite this set-back, the validation strategy as a whole is considered successful. Where facility dissociation is moderate recombination coefficients were obtained, and the first confirmation of the pressure dependency of heterogeneous catalysis has been given. The low levels of dissociation required an improvement of the experimental data reduction technique, and so consequently the error margins on the technique are reduced. While the CFD model remains unvalidated via the intended extrapolation, an improved model now exists that correctly captures the pressure and temperature dependency of catalytic recombination. The model is calibrated with data acquired at relevant temperatures on LEO relevant materials; the confidence in the model is, therefore, good.

The application of the strategy outlined in this work could be useful in future campaigns for characterising material catalytic efficiency where higher surface temperatures are important. It is acknowledged that for LEO entries, the experimental test set-up needs redesigning to permit higher enthalpy to be used. This might be achieved with a cooled sample (removing the radiative equilibrium approximation in the CFD), or perhaps via measurements on samples angled into the flow to reduce the heating.

Extended experimental characterisation could also be considered to reduce the uncertainties in the new data reduction method. This includes optical characterisation of the flow and surface conditions, determination of atomic partial pressures at the surface, post-test emissivity determination, and non-equilibrium boundary-layer treatment.

Validation of the CFD model might come from an extension of the present work by incorporating the suggestions given above for future work to acquire the necessary data, or alternatively making use of the data of other authors at higher pressure (for example the work of Panerai et al [17]). Validation from flight data is hopeful; however, it is not known whether EXPERT will fly. The Intermediate eXperimental Vehicle (IXV), which recently flew successfully, has a C-SiC composite as part of the TPS system. It is, however, not clear whether the current model calibration can be applied to families of materials (e.g. Inconel may require a different calibration to PM1000), and so this also remains to be tested in future work.

References

1. Eley, D., Rideal, E.: Parahydrogen conversion on tungsten. Nature **146**, 401–402 (1940). doi:10.1038/146401d0
2. Fatemi, J.: Metallic thermal protection system for the expert re-entry vehicle: Modelling and analysis.In: K. Fletcher (ed.) Thermal Protection Systems and Hot Structures, Proceedings of the 5th European Workshop held 17–19 May, 2006 at ESTEC, Noordwijk, The Netherlands, ESA Special Publication, vol. 631, pp. 39.1–39.8. European Space Agency (2006)
3. Fertig, M.: Finite rate surface catalysis modelling of pm1000 and sic employing the dlr cfd solver tau. In: 8th European Symposium on Aerothermodynamics for Space Vehicles, ESA Special Publ. (2015)
4. Fertig, M., Frühauf, H.H., Auweter-Kurtz, M.: Modelling of reactive processes at SiC surfaces in rarefied nonequilibrium airflows. AIAA-Paper 2002–3102, 8th AIAA Joint Thermophysics and Heat Transfer Conference, St. Louis, Missouri, USA (2002)
5. Fertig, M., Herdrich, G., Auweter-Kurtz, M.: SiO_2 catalysis modeling for CFD calculations. AIAA-Paper 2007–4257, 39th AIAA Thermophysics Conference, Miami, Florida, USA (2007)
6. Fertig, M., Herdrich, G., Auweter-Kurtz, M.: SiC oxidation and catalysis modelling for re-entry heating predictions. In: H. Lacoste, L. Ouwehand (eds.) Sixth European Symposium on Aerothermodynamics for Space Vehicles, ESA Special Publication, vol. 659 (2009)
7. Goulard, R.: On catalytic recombination rates in hypersonic stagnation heat transfer. Jet Propulsion **28**(11) (1958)
8. Herdrich, G., Fertig, M., Petkow, D., Steinbeck, A., Fasoulas, S.: Experimental and numerical techniques to assess catalysis. Prog. Aerospace Sci. **48–49**, 27–41 (2012). doi:10.1016/j.paerosci.2011.06.007
9. Hinshelwood, C.: The Kinetics of Chemical Change. At The Clarendon Press (1940). https://archive.org/details/kineticsofchemic030965mbp
10. Kim, Y.C., Boudart, M.: Recombination of o, n and h atoms on silica: Kinetics and mechanism. Langmuir **7**, 2999–3005 (1991)
11. Kolesnikov, A.F., Gordeev, A.N., Vasilevskii, S.A.: Capabilities of RF-Plasmatron IPG-4 for Re-entry Simulation J. Tech. Phys. 50(3), 181–198, Polish Academy of Sciences. Institute of Fundamental Technological Research, Warszawa (2009)
12. Langmuir, I.: The mechanism of the catalytic action of platinum in the reactions $2CO + O_2 = 2CO_2$ and $2H_2 + O_2 = 2H_2O$. Trans. Faraday Soc. **17**, 621–654 (1922). doi:10.1039/TF9221700621
13. Löhle, S., Steinbeck, A., Herdrich, G., Fasoulas, S.: Comparison of local enthalpy measureemnts using a mass injection probe with properties deduced from optical diagnostics in a pure oxygen plasma flow AIAA-paper 2011–4033, 42nd AIAA Thermophysics Conference. Honolulu, Hawaii (2011)
14. Massuti-Ballester, B., Herdrich, G.: Experimental determination of PM1000 and CVD-C/SiC catalytic properties. In: 8th European Symposium on Aerothermodynamics for Space Vehicles (2015)
15. Massuti-Ballester, B., Herdrich, G.: Surface Coverage and Pressure Dependent Catalysis of Copper. In: 30th International Symposium on Space Technology and Science (2015)
16. Massuti-Ballester, B., Pidan, S., Herdrich, G., Fertig, M.: Recent catalysis measurements at IRS. Adv. Space Res. (2015). doi:10.1016/j.asr.2015.04.028
17. Panerai, F., Marschall, J., Thömel, J., Vandendael, I., Hubin, A., Chazot, O.: Air plasma-material interactions at the oxidized surface of the PM1000 nickel-chromium superalloy. App. Surface Sci. **316**, 385–397 (2014)
18. Pidan, S.: Entwicklung eines katalyzitätsbasierten Sensorsystems für Wiedereintrittsflugkörper. Ph.D. thesis, Universität Stuttgart (2010). (in German)
19. Scott, C.D.: Catalytic recombination of oxygen and nitrogen in high temperature reusable surface insulation. AIAA-Paper

80–1477, 15th AIAA Thermophysics Conference, Snowmass, CO, USA (1980). doi:10.2514/6.1980-1477
20. Stewart, D.A.: Determination of surface catalytic efficiency for thermal protection materials - room temperature to their upper use limit. AIAA-Paper 96–1863, 31st Thermophysics Conference, New Orleans, LA (1996)
21. Stewart, D.A.: Surface catalysis and characterization of proposed candidate TPS for access-to-space vehicles. Tech. Rep. NASA TM-112206, NASA (1997)
22. Stewart, D.A., Bouslog, S.: Surface characterization of candidate metallic TPS for RLV. AIAA-Paper 99–3458, 33rd Thermophysics Conference, Norfolk, VA (1999)
23. Zoby, E.: Analysis of STS-2 experimental heating rates and transition data. In: IAA/ASME 3rd Joint Thermophysics, Fluids, Plasma and Heat Transfer Conference; AIAA82-0822 (1982)
24. Zoby, E.: Approximate heating analysis for the windward-symmetry plane of shuttle-like bodies at large angle-of-attack. Thermophy. Atmos. Entry **82**, 229 (1982)